JOURNAL OF Applied Polymer SCIENCE

Polypropylene nanocomposites with electrical and magnetic properties

Muhammad Nisar,[1] Maria da Graça Sebag Bernd,[2] Luiz C. P. da Silva Filho,[2] Julian Geshev,[3] Nara R. de Souza Basso,[4] Griselda Barrera Galland [1]

[1]Instituto de Química, Universidade Federal do Rio Grande do Sul, Avenue Bento Gonçalves 9500 91501-970, Porto Alegre Rio Grande do Sul, Brazil

[2]Laboratório de Ensaios e Modelos Estruturais, Escola de Engenharia Civil, Universidade Federal do Rio Grande do Sul, Avenue Bento Gonçalves 9500 91501-970, Porto Alegre Rio Grande do Sul, Brazil

[3]Instituto de Física, Universidade Federal do Rio Grande do Sul, Avenue Bento Gonçalves 9500 91501-970, Porto Alegre Rio Grande do Sul, Brazil

[4]Faculdade de Química, Pontifícia Universidade Católica do Rio Grande do Sul, Avenue Ipiranga 6681 90619-900, Porto Alegre Rio Grande do Sul, Brazil

Correspondence to: G. B. Galland (Email: griselda.barrera@ufrgs.br)

ABSTRACT: The magnetic and conducting properties of polypropylene (PP)–reduced graphene oxide (rGO)–carbon nanotube with iron (CNT-Fe) nanocomposites prepared by melt mixing were studied. CNT-Fes were synthesized by the pyrolysis of sawdust, and rGO was produced from graphite flakes. The combination of these two materials was used to produce magnetic and conducting properties in a diamagnetic and insulating PP matrix with the addition of a small amount of filler. A constant and minute amount of CNT-Fes was sufficient to introduce magnetic characteristics to the PP matrix. A variable amount of rGO was used, and the percolation threshold was achieved with the use of only 2.1 wt % rGO. All samples reached magnetic saturation at about 4.2 kOe, with an identical coercivity of 150 Oe and a normalized remnant magnetization of 0.14. Thermogravimetric and differential scanning calorimetry analyses showed enhancements in the maximum degradation temperature, melting temperature, crystallization temperature, and crystallinity. The nanocomposites showed better mechanical and barrier properties than the neat polymer. The novelty of this study was the use of a filler derived from waste combined with rGO to obtain a thermoplastic nanocomposite with both magnetic and conducting properties at room temperature. © 2018 Wiley Periodicals, Inc. J. Appl. Polym. Sci. **2018**, *135*, 46820.

KEYWORDS: magnetism and magnetic properties; mechanical properties; polyolefins; thermoplastics

Received 1 March 2018; accepted 29 May 2018
DOI: 10.1002/app.46820

INTRODUCTION

Polymer nanocomposites with advanced thermal stability, flame retardancy, mechanical properties, electrical conductivity, magnetic properties, and/or chemical resistance, depending on the type of filler used, have shown increasing scientific significance.[1–3] There have been incredible enrichments in the properties of polymers with the incorporation of minute amounts of fillers, for instance, carbon nanotubes (CNTs), exfoliated nanosilicate layers, and graphite nanoplatelets. However, a well-built interfacial adhesion within the polymer matrix and the nanosized filler and also a uniform dispersion of the filler in the polymer matrix are necessary for the efficient performance of these fillers.[4]

CNTs were first reported by Iijima in 1991.[5] In 1994, Ajayan *et al.*[6] reported the first polymeric material with CNTs as nanofillers. The outstanding combination of mechanical, electrical, and thermal properties, high flexibility, and low mass density of the CNTs make them exceptional candidates to replace the usual nanofillers in a variety of fields.[7–12] The various techniques used to produce CNTs include electric arc discharge, laser ablation, and chemical vapor deposition (CVD).[13] The use of CVD techniques is considered the most suitable method for large-scale CNT production.[14] More recently, Filho and coworkers[15,16] have developed a low-cost CVD method for the production of CNTs with the pyrolysis of waste wood sawdust as a carbon source. The process is important because it also creates an environmental demand because it also produces hydrogen. Wood sawdust was mixed with a reducing agent (commercial zinc), calcite (bed material), and a catalyst {ferrocene [$Fe(C_5H_5)_2$] or Fe/Mo/MgO} arranged in a column reactor and then heated to 750 °C for 3 h without blowing air. The presence of iron in the CNTs makes them suitable for magnetic applications.

The discovery of graphene, a monolayer of sp^2-hybridized carbon atoms, has attracted attention and spurred a new area of research in polymer composites because of its tremendous thermal, mechanical, and electrical properties.[17] These properties make graphene an excellent material for improving the properties of neat polymers.[18] Common methods used to produce graphene include CVD, CO reduction, and the exfoliation of graphite. The latter method is considered a suitable technique for the production of large quantities of graphene with affordable costs and is the one used to produce nanocomposites.[19]

Polypropylene (PP) is commercially a very important polyolefin because of its low cost; inertness toward acids, alkalis, and solvents; high stiffness; and good tensile strength. However, it is imperative that one enhance the properties of PP for advanced applications.[20] The mechanical properties of PP can be improved by the incorporation of various fibers and fillers. Recently, to improve the electrical conductivity, thermal conductivity, and barrier properties, the production of PP–graphene and PP–CNT nanocomposites have been reported.[21–23] Various methods have been used to produce nanocomposites: solution mixing,[24] *in situ* polymerization,[25] and melt blending.[26–29] However, there are limitations of solution mixing in the case of PP and polyethylene because these polymers are soluble in solvents, such as xylene and trichlorobenzene, only above 120 °C; this can cause serious health risks.[4] *In situ* polymerization is not suitable for large-scale production. Melt mixing is one of the most used techniques because of its simplicity, high yield, fast production, easy operation, and the fact that it does not need a hazardous solvent that could cause health problems.[30]

Multifunctional magnetic polymer composites can be used in various fields, such as in microwave absorbers, biomedicine, magnetic recording materials, information technology, energy storage devices, magnetic resonance imaging, magnetic sensors, catalysis, drug delivery, telecommunications, and environmental remediation.[26,31–33] Magnetic polymer nanocomposites can be obtained by the introduction of a range of magnetic elements, such as iron, nickel, and cobalt, in a diamagnetic polymer matrix with different polymerization techniques.[34] Although iron is a conventionally used magnetic material,[35] the easy oxidation of iron NPs is a hot topic of discussion when NPs are used as fillers in polymer matrixes. NPs have a tendency to agglomerate to decrease the energy related to their high surface areas. The chemical stabilization of the magnetic constituent is achieved by coating with silica or carbon to prevent aggregation.[36] The encapsulation of iron NPs in CNTs synthesized by the CVD method, where $Fe(C_5H_5)_2$ is used as a catalyst and precursor of synthesis, is considered a suitable strategy.[37–39] In recent studies, we obtained polyethylene and PP–carbon nanotube with iron (CNT-Fe) nanocomposites with good magnetic properties at room temperature using CNT-Fes synthesized from $Fe(C_5H_5)_2$ by CVD and *in situ* polymerization for the production of nanocomposites.[40–42]

In this study, we aimed to produce a dual-stimuli-responsive material under electrical and magnetic fields (*H*s) at room temperature using reduced graphene oxide (rGO) to introduce a conductive network in the isolated PP matrix and CNT-Fe to introduce the magnetic properties. The CNT-Fes were obtained from sawdust via a process developed by Filho *et al.*[15] PP–rGO–CNT-Fe nanocomposites were fabricated with the melt-mixing technique and commercial PP. These multifunctional materials can be used in different industrial applications, including in medical sensors, electronic devices, low-temperature heaters, energy-storage devices, solar cells, magnetic recording materials, magnetic sensors, and microwave absorbers, and in the aerospace and automotive industries.[43–46]

EXPERIMENTAL

Commercially isotactic polypropylene (iPP; PP2621), provided by Petroquim S. A. (Hualpén, Chile), was used as the polymer matrix. iPP had the following characteristics: melt flow rate- = 26 g/10 min (2.16 kg/230 °C; Norm ASTM D 1238/95), weight-average molecular weight = 195 kg/mol, number-average molecular weight = 71 kg/mol, polydispersity index = 2.72, and melting temperature (T_m) = 160 °C. Irganox 1010 was used as an antioxidant agent during the composite preparation.

CNT Synthesis

Sawdust from the furniture industry was gathered as a raw material for the synthesis of the CNTs with a reported method.[19] Commercially available zinc served a reducing agent. $Fe(C_5H_5)_2$ was used as a catalyst for they synthesis. The method of synthesis is elaborated in detail in refs. 15 and 16.

Graphene Oxide Synthesis and Thermal Reduction

A modified Staudenmaier method was used to synthesize graphene oxide from flakes.[47,48] The graphite oxide was heated up to 600 °C for 3 s in an oven to obtain rGO under a normal atmosphere in a closed quartz ampule. The amount of oxygen calculated by elemental analysis was 27%. The complete characterization of the rGO can be found in ref. 48.

Filler Composition

Three filler compositions (GCFe = rGO + CNT-Fe), $GCFe_1$ (2.0 wt %), $GCFe_2$ (2.6 wt %), and $GCFe_3$ (3.1 wt %), were used. These fillers were composed of a mixture of a constant amount of CNT-Fes (1.0 wt %) and a variable amount of rGO (1.0, 1.6, or 2.1 wt %, respectively).

Melt Compounding

For the preparation of the composites, a melt mixer (Brabender Plasticorder, Diusburg, Germany), operating at 190 °C at a speed of 110 rpm, was used. Calculated amounts of iPP and rGO–CNT-Fes and a small amount (~0.005 g) of Irganox 1010 as an antioxidant were used for mixing, with the total accumulated amount being about 30 g. The amount of filler was varied from 0 to 3.1 wt %. The iPP was first mixed with the antioxidant, and subsequently, half the amount of the polymer (~13 g) was added to the mixer, which was operated at 110 rpm. After 2 min, the filler was added to the melted polymer for 3 min. In the last step, the rest of the polymer pellets were added, and the speed of the mixer was kept constant at 110 rpm for 10 min. The total mixing time was about 15 min.

Characterization

The thermal properties were measured with differential scanning calorimetry (DSC) with a Perkin-Elmer differential calorimeter (model DSC Q20). The temperature was increased from 0 to 180 °C at 10 °C/min then maintained at 180 °C for 2 min, and cooled down to 40 °C at 10 °C/min. Finally, a DSC scan was recorded at 10 °C/min to determine T_m. The crystallinity (X_c) values were calculated from the enthalpy of fusion with 207 J/g for 100% crystalline PP.[49,50]

Thermogravimetric analysis, performed with an SDT Q600 thermal analyzer (Q20, TA Instruments, New Castle, DE), was used to study the thermal stability of the nanocomposites with respect to the neat polymer. The samples were scanned in the range of 0 to 800 °C at a scanning rate of 20 °C/min.

The morphologies of the nanoparticles (CNT-Fe) and rGO were investigated with scanning electron microscopy (SEM; JEOL JSM 6500F) and transmission electron microscopy [TEM; JEOL (JEM-2010, operating at 200 kV)]. SEM (Phillips XL30, operating at 20 kV) was used to examine the nanocomposites. The samples were deposited on an aluminum stub and coated with gold. The nanocomposites (iPP–rGO–CNT-Fe) were also analyzed with TEM (JEOL 1011, operating at 120 kV). Ultrathin films (~50 nm thick) cut under cryogenic conditions with a Leica Ultracut UCT microtome at −70 °C placed on a grid were used to prepare the samples.

An HP model D-500 dynamometer at about 25 °C was used to measure the mechanical properties according to ASTMD638-10. Five samples were tested for each weight percentage nanocomposite, and the results were the average value of these five measurements. The bone-shaped samples had an overall length of 120 mm with a distance between the two grips of 80 mm, a width of 11.5 mm, and a thickness of 1 mm at the crosshead. A rate of 50 mm/min was tested.

A megohmmeter (Megger BM11) operating at a maximum voltage of 1200 V was used to measure the electric resistivity. A standard two-point method was used with this setup. For each electrical value presented in this contribution, at least four samples were prepared, and four measurements were carried out for each one. In general, differences of around one order of magnitude were detected in the nonpercolated samples with low conductivity values (~10^{-9} S/cm). For the percolated samples, the experimental error for the conductivities was less than 50%. The samples prepared for this test were $40 \times 15\ mm^2$ with a thickness of 1 mm.

The oxygen permeability was measured with an L100-5000 permeability instrument manufactured in the United Kingdom connected to a vacuum pump and a cooling and heating bath to control the temperature. The tolerance in percentage to equilibrium was 2, and the oxygen pressure was maintained at 5 bar. Three measurements were obtained for each sample, and the results were the average of these three measurements.

The water contact angle (WCA) test was carried out with the sessile drop method, where drops of 2 μL of deionized water at room temperature was steadily deposited on the surface of the neat PP matrix and its nanocomposites with a microsyringe. The images were captured with drop shape analysis system equipment (Kruss, DSA). Each measurement was repeated at least five times at different positions. A digital video camera was used to capture the images, which were analyzed by Surftens 3.0 software for contact angle measurements.

An EZ9MicroSense vibrating sample magnetometer was used at room temperature with H cycled between −20 and 20 kOe to investigate the magnetic properties of the nanocomposites.

Table I. Thermal Properties of the PP–rGO–CNT-Fe Nanocomposites

Sample	Filler (%)[a]	T_c (°C)	T_m (°C)	X_c (%)	T_{onset} (°C)	T_{max} (°C)
PP	0	112	158	59	427	470
PP-CFe_1	2.0	122	162	60	455	475
PP-$GCFe_2$	2.6	122	162	65	453	486
PP-$GCFe_3$	3.1	123	162	63	458	488

[a] Filler = GCFe = rGO + CNT-Fe.

RESULTS AND DISCUSSION

Thermal Analysis

Table I shows the DSC results of the neat PP and its nanocomposites. With the introduction of the filler, increases of 11 °C were observed in the crystallization temperature (T_c); this demonstrated that the filler acted as a nucleating agent. T_m increased 4 °C, and X_c also showed an increase of 6% compared to that of the neat PP. This suggested that bigger or more perfect crystals were formed.

The variation in the stability of the polymers with the incorporation of the rGO–CNT-Fes (CGFe) was determined with thermogravimetric analysis. Table I gives the results of a number of the nanocomposites with filler contents ranging from 0 to 3.1 wt %. The amount of filler was determined from the amount added to the mixture and the polymer yield. As shown in Table I, the initial degradation temperature (T_{onset}) and maximum degradation temperature (T_{max}) increased 31 and 18 °C, respectively, as the filler concentration increased. The enhancement in the thermal stability of the polymer was mostly attributed to the formation and stabilization effect of the filler-bonded macroradicals and filler barrier effect.[51]

Morphologies of the Nanocomposites

Figure 1 gives the scanning electron micrographs of the fractured surface of the neat PP and its nanocomposites with different weight percentages of rGO–CNT-Fes. The samples were first cooled in liquid nitrogen and then broken without deformation. SEM of the CNT-Fe and rGO nanoparticles are also shown. The rGO–CNT-Fes seemed to be well distributed in the PP matrix, where no agglomerates were observed. When the concentration of the filler was increased, a more layered structure of the polymer matrix appeared; this showed strong interactions between the filler and the polymer matrix.

The TEM morphological evaluation of the nanocomposites was carried out to determine the morphology and dispersion of the filler in the polymer matrix. Figure 2 shows TEM images of the

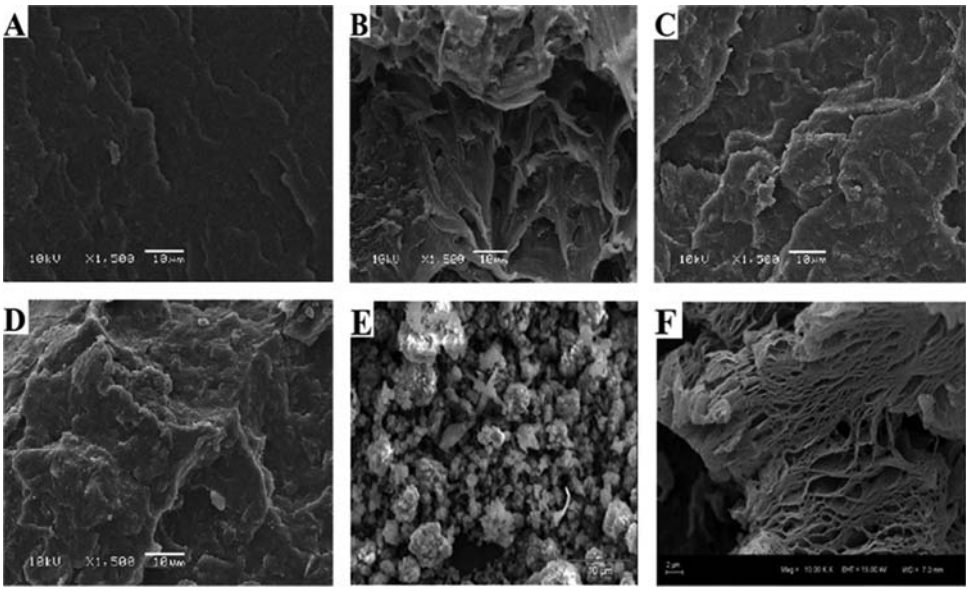

Figure 1. SEM images: (A) neat PP; PP–rGO–CNT-Fe nanocomposites with (B) 2.0, (C) 2.6, and (D) 3.1 wt % filler; (E) CNT-Fe; and (F) rGO.

CNT-Fes [Figure 2(a)], rGO [Figure 2(b)], and the PP–rGO–CNT-Fe nanocomposites with 2 wt % filler [Figures 2(c–e)] and 3.1 wt % filler [Figures (f–h)]. It is clear from the micrographs that the filler was uniformly distributed in the polymer matrix. The polymer matrix seemed to be wrapped around the filler, and no aggregation was observed. In Figure 2(e,h), an isolated CNT was observed.

Mechanical Properties

Figure 3(a,b) demonstrates the effects of the filler on the Young's modulus and elongation at break. It is clear from the results that with the incorporation of only 2.6% filler, an increase of about 13% (183 MPa) was observed; this reached a higher value of about 22% (314 MPa) with the incorporation of 3.1% filler. This enhancement in the modulus was attributed to the uniform dispersion of the filler in the polymer matrix and an effective load transfer from the filler to the matrix due to strong interfacial adhesion.[4] The results show the improvement of the material's rigidity as a result of the filler loading.[52] A similar enhancement in the Young's modulus was shown by Song *et al.*[4] and Hunang *et al.*[53] for PP–graphene nanocomposites.

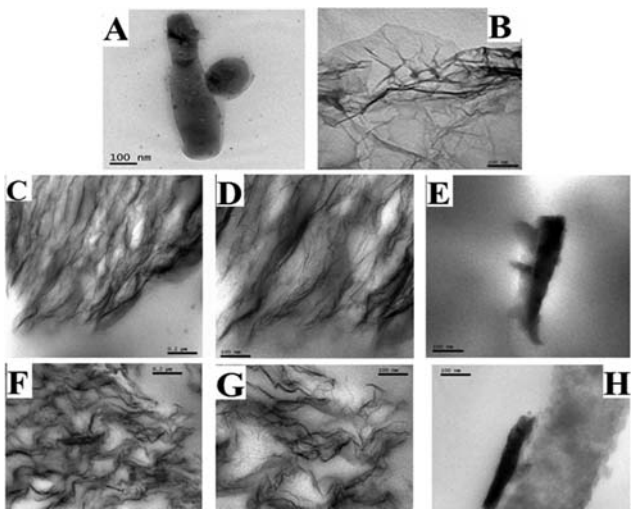

Figure 2. TEM images: (A) CNT-Fe (bar = 100 nm); (B) rGO (bar = 100 nm); 2 wt % PP–rGO–CNT-Fe nanocomposites with bar = (C) 0.2 μm, (D) 100 nm, and (E) 100 nm; and 3.1 wt % PP–rGO–CNT-Fe nanocomposites with bar = (F) 0.2 μm, (G) 100 nm, and (H) 100 nm.

The results of the elongation at the break point measurement are presented in Figure 3(b). We observed that with an increase in the filler from 2.6 to 3.1%, decreases of 37 and 50%, respectively, occurred in the elongation at break compared to that of neat PP. A similar decreasing tendency in the elongation at break for graphene–PP nanocomposites were reported by other researchers.[54,55]

Electrical Conductivity

The transformation of PP, which is an insulating material, to a semiconductor can broaden the industrial applications of this polymer. The formation of a conductive network of a filler and the transformation of an insulating material to a semiconductor are achieved only when the amount of conductive filler is above the electrical percolation threshold.[56] Table II and Figure 4 show the conductivities of the neat PP and PP–rGO–CNT-Fe nanocomposites. Table II also shows the electrical conductivity results of the polyethylene–graphite nanocomposites from previous works. We observed that the PP and the nanocomposites up to 2.6 wt % CGFe still remained insulating. A significant drop in the electrical resistivity was observed as when the filler amount was increased to 3.1 wt %. This indicated that the electrical percolation threshold fell between 2.6 and 3.1 wt % and the crosslinking network structure of naturally conductive rGO was formed; this was the main source of conductivity in this study. Li *et al.*[57] reported electrical percolations between 8 and 12 wt % for PP–graphene nanoplatelet nanocomposites. The amount we incorporated was almost three times lower than theirs. This improved conductivity was attributed to the good exfoliation of rGO.[58]

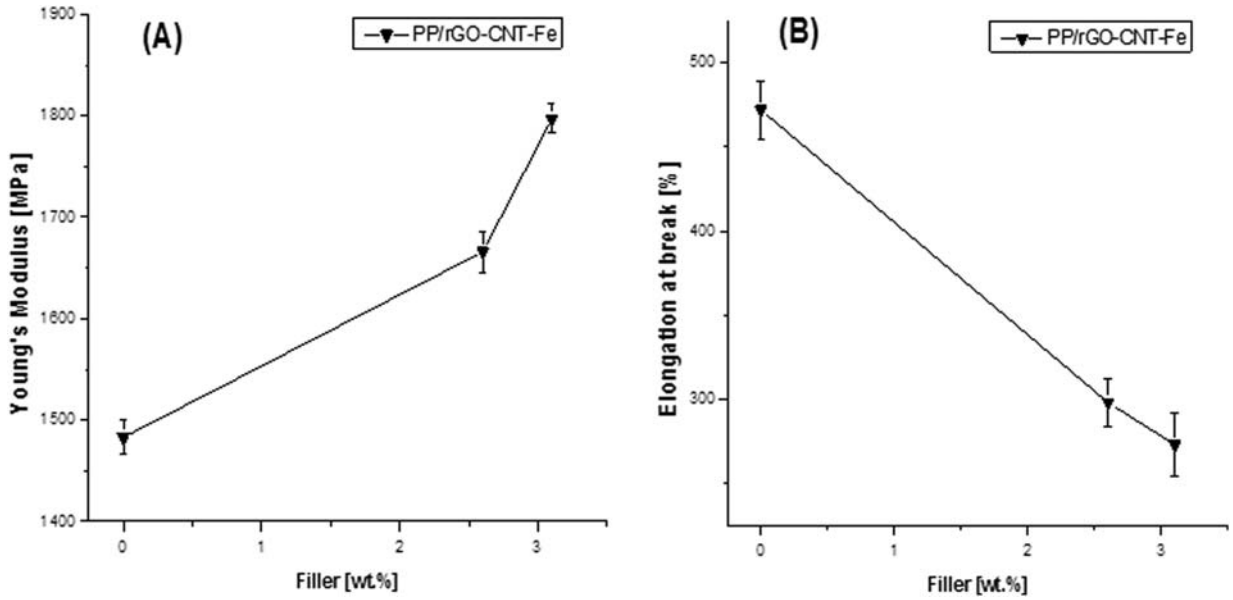

Figure 3. (A) Modulus and (B) elongation at break of the neat PP and PP–rGO–CNT-Fe nanocomposites.

In our recent work, with the same graphene obtaining polyethylene–rGO–CNT-Fe nanocomposites by *in situ* polymerization, we obtained a conductivity of 4.99×10^{-6} S/cm with 2.4% graphene; this was very similar to these results.[41] Previous studies[19] showed that rGO was more exfoliated than graphite nanosheets and had fewer graphene layers per sheet; when graphite nanosheets were used to obtain polyethylene nanocomposites by *in situ* polymerization, conductivity was observed only when a higher amount of filler (15.3 wt %) was used. The differences in the type of graphite used had a remarkable influence on the conductivity of the composite materials obtained.

Oxygen Barrier Properties

The permeability of polymers to gases and liquids has been an area of growing scientific interest for many years, as it is an important property on the basis of which a material can be evaluated for a range of industrial applications. Gas barrier materials have potential for applications in the field of packaging materials and electronic and medical applications.[59] To improve the barrier properties of plastic materials, two common techniques are used: surface coating or the introduction of nanoparticles to form nanocomposites, as we did in this study.[60] Table II and Figure 5 demonstrate the effect of the filler percentage on the permeability to oxygen at 23 °C for the neat PP films and their nanocomposites with thicknesses of about 0.25 mm. We observed that with the addition of the filler, the permeability decreased steadily up to 30% with the addition of only 2 wt % filler and decreased to a higher value, about 50%, with the incorporation of 3 wt % filler. Polymer permeability to gases is normally influenced by two factors: an increase in X_c and the presence of a filler. iPP contains both crystalline and amorphous regions; the gas permeability in the crystalline region is considered negligible, and the permeation of the gas takes place only in the amorphous region. As supported by our DSC results, X_c increased with the incorporation of the filler[61] because of the fact that the rGO and CNTs acted as nucleating agents for the PE and PP matrix.[19,41,51] The nanocomposites were considered a multiphase system in which the existence of

Table II. Contact Angle, Conductivity, and Oxygen Permeability Values of the PP–rGO–CNT-Fe Nanocomposites

Sample	rGO (wt %)	CNT-Fe (wt %)	WCA (°)	Conductivity (S/cm)	Oxygen permeability at 0% RH (mL/m^2 × 24 h)
PP	0.0	0.0	107.3 ± 0.2	5.6×10^{-11}	52.0
PP-GCFe$_1$[a]	1.0	1.0	107.4 ± 0.3	8.3×10^{-11}	36.3
PP-GCFe$_2$[a]	1.6	1.0	111.5 ± 0.2	7.5×10^{-11}	29.0
PP-GCFe$_3$[a]	2.1	1.0	109.4 ± 0.1	2.3×10^{-8}	27.3
PE-GCFe[b]	2.4	0.46	—	4.99×10^{-6}	—
PErGO[c]	2.2	—	—	8.5×10^{-8}	—
PEGNS[c]	15.3	—	—	1.6×10^{-7}	—

RH, relative humidity; PE, Polyethylene; PErGO, Polyethylene/reduced graphene oxide; PEGNS, Polyethylene/graphite nanosheets
[a] Filler = GCFe = rGO + CNT-Fe.
[b] Data from ref. 41.
[c] Data from ref. 19.

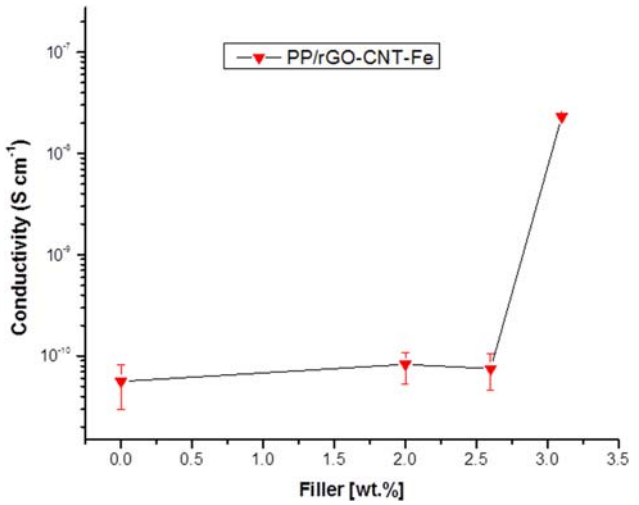

Figure 4. Electrical conductivity of the neat PP and PP–rGO–CNT-Fe nanocomposites. [Color figure can be viewed at wileyonlinelibrary.com]

different phases, crystalline, inorganic, and amorphous, caused complex phenomena on the procedure of gas permeation. The presence of the rGO–CNT-Fe filler introduced a more limited path for the gas molecules to pass through the polymer. The reduction in the penetrability was clear from the experimental results and was due the existence of the more tortuous path, apart from the crystalline region, which was comparatively less permeable, as the gas molecules had to pass through the filler, which was considered impermeable.[61]

Contact Angle Study

For advanced applications of the composite materials, a knowledge of the affinity toward water is an important parameter. To be considered superhydrophobic, the surface has to exhibit high WCAs (>150 °).[62] Table II shows the WCA results; with the addition of the filler, a slight increase in the angle was observed. This demonstrated an improvement in the hydrophobic nature of the material.

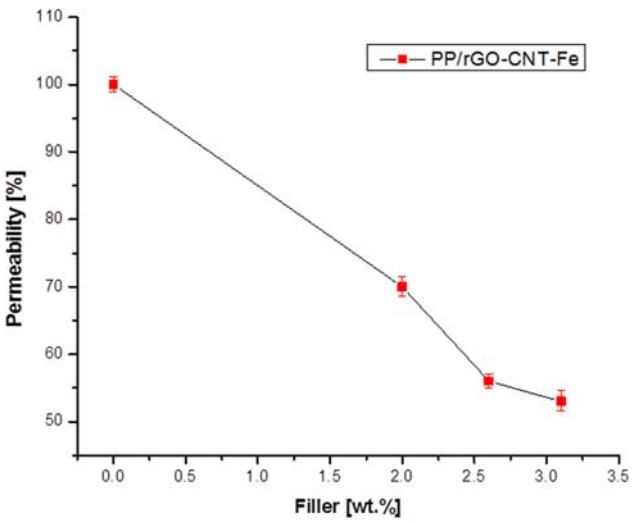

Figure 5. Effect of the filler (wt %) on the permeability of the nanocomposites toward oxygen. [Color figure can be viewed at wileyonlinelibrary.com]

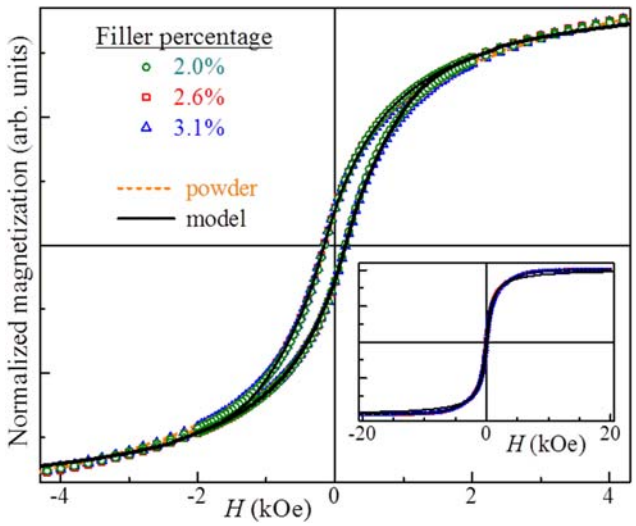

Figure 6. Low-field magnetization hysteresis loops traced at room temperature for the PP–rGO–CNT-Fe nanocomposites with different filler contents together with that traced on the powder. The solid line is a model one obtained with the assumption that the system consisted of both ferromagnetic and SPM single-domain particles. The inset presents the whole-field-range loops. [Color figure can be viewed at wileyonlinelibrary.com]

Magnetic Properties

The normalized (to their respective saturation values) magnetization hysteresis loops of the PP–rGO–CNT-Fe nanocomposites and that of the powder (filler), traced at room temperature, are shown in Figure 6. A diamagnetic correction was applied on each measured curve. We also ensured that the magnitude of the maximum H used was high enough to prevent minor loop effects.[63–66] As shown, all of the loops were practically identical, with a normalized remnant magnetization of 0.14 and a coercivity equal to 150 (±2) Oe. All of the curves were effectively saturated above about 4.2 (±0.1) kOe. We concluded that in contrast to the other properties, the magnetic ones did not change from those of the starting magnetic material when it was used as a filler and introduced into the polymer matrix.

At sufficiently high temperatures, the magnetic moments of very small particles are thermally agitated so they can rotate to their equilibrium directions. Such particles are called superparamagnetic (SPM). Here, we considered that our samples contained two magnetic phases: (1) noninteracting SPM particles and (2) stable (interacting small and/or larger ferromagnetic) grains, and we performed numerical simulations that allowed us to estimate the average sizes (Ds) of the SPM particles by fitting the experimental hysteresis loops with a method described elsewhere.[67,68] The solid line in Figure 6 was calculated with the assumption of a system of randomly oriented, single-domain, uniaxial anisotropy particles with a Gaussian distribution of the SPM D of 3.8 nm and a standard deviation equal to 1.8 nm.

CONCLUSIONS

Nanocomposites made from PP–rGO and CNT-Fes produced from wood sawdust from the furniture industry were obtained. The synthesized materials showed improvements in their thermal stability and higher T_cs than those of PP. Nanocomposites

with only 3.1 wt % filler presented a reduction in oxygen permeability of 50% and an enhancement of 22% (314 MPa) in the Young's modulus. The obtained CNTs had magnetic properties because of the use of a catalyst containing iron. The room-temperature magnetization hysteresis showed that the nanocomposites consisted of both ferromagnetic and SPM parts with a very low percentage of filler. The value of the room-temperature coercivity shown by the nanocomposites was a rather remarkable result given that most research in this area has reported materials that are magnetic only at very low temperatures.[69] The conductivity results from the presence of rGO, which formed a conducting network in the polymer matrix. We obtained our objective of obtaining a dual-stimuli-responsive material under electrical fields and *H*s at room temperature with rGO and a nanoparticle (CNT-Fe) from waste. Other properties, such as thermal stability, elastic modulus, and permeability to oxygen, were enhanced compared to those of neat PP; this will broaden the applications of this material.

ACKNOWLEDGMENTS

The authors are grateful to the The World Academy of Sciences - Conselho Nacional de Desenvolvimento Científico e Tecnológico (TWAS-CNPq) for the fellowship to Muhammad Nisar (contract grant number 3240274293) and to Conselho Nacional de Desenvolvimento Científico e Tecnológico (CNPq) for grant 302902/2013-9. They thank Raúl Quijada from the University of Chile for the support. They also thank Centro de Microscopia e Microanálise (CMM) and Laboratório Regional de Nanotecnologia (LRNANO) from Universidade Federal do Rio Grande do Sul (UFRGS) for microscopy analysis. The magnetic characterization was performed in collaboration with the Laboratory of Magnetism at Instituto de Física-Universidade Federal do Rio Grande do Sul (IF-UFRGS).

There are no conflicts of interest to declare.

REFERENCES

1. Jancar, J.; Douglas, J. F.; Starr, F. W.; Kumar, S. K.; Cassagnau, P.; Lesser, A. J.; Sternstein, S. S.; Buehler, M. *Polymer* **2010**, *51*, 3321.
2. Jeon, I. Y.; Baek, J. B. *Materials* **2010**, *3*, 3654.
3. He, Q.; Yuan, T.; Zhu, J.; Luo, Z.; Haldolaarachchige, V.; Sun, L.; Khasanov, A.; Li, Y.; Young, D. P.; We, S.; Guo, Z. *Polymer* **2012**, *53*, 3642.
4. Song, P.; Cao, Z.; Cai, Y.; Zhao, L.; Fang, Z.; Fu, S. *Polymer* **2011**, *52*, 4001.
5. Iijima, S. *Nature* **1991**, *354*, 56.
6. Ajayan, P. M.; Stephan, O.; Colliex, C.; Trauth, D. *Science* **1994**, *265*, 1212.
7. Cooper, C. A.; Young, R. J.; Halasll, M. *Compos. A* **2001**, *32*, 401.
8. Gao, G.; Cagin, T.; Goddard, W. A., III. *Nanotechnology* **1998**, *9*, 184.
9. Moniruzzaman, M.; Winey, K. I. *Macromolecules* **2006**, *39*, 5194.
10. Treacy, M. M. J.; Ebbesen, T. W.; Gibson, J. M. *Nature* **1996**, *381*, 678.
11. Reddy, K. R.; Sin, B. C.; Yoo, C. H.; Sohn, D.; Lee, Y. *J. Colloid Interface Sci.* **2009**, *340*, 160.
12. Lau, A. K. T.; Hui, D. *Compos. B* **2002**, *33*, 263.
13. Ramesh, P.; Okazaki, T.; Sugai, T.; Kimura, J.; Kishi, N.; Sato, K.; Ozeki, Y.; Shinohara, H. *Chem. Phys. Lett.* **2006**, *418*, 408.
14. Mubarak, N. M.; Abdullah, E. C.; Jayakumar, N. S.; Sahu, J. N. *J. Ind. Eng. Chem.* **2014**, *20*, 1186.
15. Bernd, G. S.; Braganca, S. R.; Heck, N.; Luiz, C. P.; Filho, D. S. *J. Mater. Res. Technol.* [Online] **2017**. https://doi.org/10.1016/j.jmrt.2016.11.003.
16. Filho, S.; Luiz, C. P.; Heck, N. C.; Bernd, M. G. S. *Brazil. Pat. BR* 10 022053-9 A2 (**2012**). http://hdl.handle.net/10183/107424.
17. Potts, J. R.; Dreyar, D. R.; Bielawski, C. W.; Rouff, R. S. *Polymer* **2011**, *52*, 5.
18. Wakabayashi, K.; Pierre, C.; Dikin, D. A.; Rouff, R. S.; Ramanathan, T.; Brinson, L. C.; Torkelson, J. M. *Macromolecules* **2008**, *41*, 1905.
19. Pavoski, G.; Maraschin, T.; Milani, M. A.; Azambuja, D. S.; Quijada, R.; Moura, C. M.; Basso, N. R. S.; Galland, G. B. *Polymer* **2015**, *81*, 79.
20. An, J.; Jeon, G. *Fiber Polym.* **2012**, *13*, 507.
21. Lee, G. W.; Jagannathan, S.; Chae, H. G.; Mimus, M. L.; Kumar, S. *Polymer* **2008**, *49*, 1831.
22. Kalaitzidou, K.; Fukushima, H.; Drzal, L. T. *Carbon* **2007**, *45*, 1446.
23. Huang, Y. J.; Qin, Y. W.; Zhou, Y.; Niu, H.; Yu, Z. Z.; Dong, Y. *J. Chem. Mater.* **2010**, *22*, 4096.
24. Curran, S.; Davey, A. P.; Coleman, J.; Dalton, A.; McCarthy, B.; Maier, S. *Synth. Met.* **1999**, *103*, 2559.
25. Funck, A.; Kaminsky, W. *Compos. Sci. Technol.* **2007**, *67*, 906.
26. Riquelme, J.; Garzon, C. A.; Bergmann, C. P.; Geshev, J.; Quijada, R. *Eur. Polym. J.* **2016**, *75*, 200.
27. Potschke, P.; Bhattacharyy, A. R.; Janke, A. *Carbon* **2004**, *42*, 965.
28. Dondero, W. E.; Gorga, R. E. *J. Polym. Sci. Part B: Polym. Phys.* **2006**, *44*, 864.
29. Yasin, T.; Nisar, M.; Shafiq, M.; Nho, Y.; Ahmad, R. *Polym. Compos.* **2013**, *34*, 408.
30. Bao, S. P.; Tjong, S. C. *Mater. Sci. Eng. A* **2008**, *485*, 506.
31. Coey, J. M. D. *J. Magn. Magn. Mater.* **1999**, *196*, 1.
32. Shull, R. D.; Bennett, L. *H.; Nanostruct. Mater.* **1992**, *1*, 83.
33. Zhu, J.; Wei, S.; Chen, M.; Gu, H.; Rapole, S. B.; Pallavkar, S.; Ho, T. C.; Hopper, J.; Guo, Z. *Adv. Powder Technol.* **2013**, *24*, 459.
34. Schinteie, G.; Kuncser, V.; Palade, P.; Alexandrescu, R.; Morjan, I.; Filoti, G. *J. Alloy. Compd.* **2013**, *564*, 27.
35. Wei, S.; Wang, Q.; Zhu, J.; Sun, L.; Lin, H.; Guo, Z. *Nanoscale* **2011**, *3*, 4474.
36. Susheel, K.; Sarita, K.; Amit, K.; Yuvaraj, H.; Bandan, K.; Rajesh, K. *Colloid Polym. Sci.* **2014**, *292*, 2025.

37. Bhatia, R.; Prasad, V. *Solid State Commun.* **2010**, *150*, 311.
38. Osorio, A. G.; Bergmann, C. P. *Appl. Surf. Sci.* **2013**, *264*, 794.
39. Osorio, A. G.; Pereira, L. G.; Da Cunha, J. B. M.; Bergmann, C. P. *Mater. Res. Bull.* **2013**, *48*, 4168.
40. Nisar, M.; Bergmman, C. P.; Geshev, J.; Quijada, R.; Galland, G. B. *Polymer* **2016**, *97*, 131.
41. Nisar, M.; Bergmman, C. P.; Geshev, J.; Quijada, R.; Maeaschin, T.; Basso, N. R. S.; Barrera, E. G.; Galland, G. B. J. *Appl. Polym. Sci.* **2017**, *134*, 45382.
42. Nisar, M.; Bergmman, C. P.; Geshev, J.; Quijada, R.; Galland, G. B. *Polymer* **2017**, *118*, 68.
43. Kim, P.; Doss, N. M.; Tillotson, J. P.; Hotchkiss, P. J.; Pan, M. J.; Marder, S. R.; Li, J.; Calame, J. P.; Perry, J. W. *ACS Nano* **2009**, *3*, 2581.
44. Dai, Q.; Berman, D.; Virwani, K.; Frommer, J.; Jubert, P. O.; Lam, M.; Topuria, T.; Imaino, W.; Nelso, A. *Nano Lett.* **2010**, *10*, 3216.
45. Shimad, T.; Ookubo, K.; Komuro, N.; Shimizu, T.; Uehara, N. *Langmuir* **2007**, *23*, 11225.
46. Guo, Z.; Lee, S. E.; Kim, H.; Park, S.; Hahn, H. T.; Karki, A. B.; Young, D. P. *Acta Mater.* **2009**, *57*, 267.
47. Staudenmaier, L. *Chem. Ges.* **1898**, *31*, 1481.
48. Pavoski, G.; Maraschin, T.; Fim, F. C.; Balzaretti, N. M.; Galland, G. B.; Moura, C. S.; Basso, N. R. S. *Mater. Res.* **2017**, *20*, 53.
49. Seo, M. K.; Park, S. *J. Matter. Eng.* **2004**, *289*, 368.
50. Gopakumar, T. G.; Pagé, D. J. Y. S. *Polym. Eng. Sci.* **2004**, *44*, 1162.
51. Koval'chuk, A. A.; Shchegolikhin, A. N.; Shevehenko, V. G.; Nedorezovz, P. M.; Klyamkina, A. N.; Aladyshev, A. M. *Macromolecules* **2008**, *41*, 3149.
52. Zou, H.; Wu, S.; Shen, J. *Chem. Rev.* **2008**, *108*, 3893.
53. Huang, C. L.; Lou, C. W.; Liu, C. F.; Huang, C. H.; Song, X. M.; Lin, J. H. *Appl. Sci.* **2015**, *5*, 1196.
54. Yuan, B.; Bao, C.; Song, L.; Hong, N.; Liew, K. M.; Hu, Y. *Chem. Eng. J.* **2014**, *237*, 411.
55. Achaby, M. E.; Arrakhiz, F. E.; Vaudreuil, S. B.; Qaiss, A. K.; Bousmina, M.; Fehri, O. F. *Polym. Compos.* **2012**, *33*, 733.
56. Wongtimnoi, K.; Guiffard, B.; de Moortele, A. B.; Seveyrat, L.; Gauthiev, C.; Cavaille, J. Y. *Compos. Sci. Technol.* **2010**, *71*, 885.
57. Li, Y.; Zhu, J.; Wei, S.; Ryu, J.; Sun, L.; Guo, Z. *Macromol. Chem. Phys.* **2011**, *121*, 1951.
58. Park, J. H.; Choudhury, A.; Farmer, B. L.; Dang, T. D.; Park, S. Y. *Polymer* **2012**, *53*, 3937.
59. Hiltner, A.; Liu, R. Y. F.; Hu, Y. S.; Baer, E. J. *Polym. Sci. Part B: Polym. Phys.* **2005**, *43*, 1047.
60. Zehetmeyer, G.; Scheibel, J. M.; Soares, R. M. D.; Weibel, D. E.; Oviedo, M. A. S.; Oliveira, R. V. B. *Polym. Bull.* **2013**, *70*, 2181.
61. Vladimirov, V.; Betchev, C.; Vassiliou, A.; Papageorgiou, G.; Bikiaris, D. *Compos. Sci. Technol.* **2006**, *66*, 2935.
62. Chagas, G. R.; Weibel, D. E. *Polym. Bull.* **2017**, *74*, 1965.
63. Geshev, J. *J. Magn. Magn. Mater.* **2008**, *320*, 600.
64. Geshev, J. *Appl. Phys. Lett.* **2008**, *93*, 176101.
65. Geshev, J.; Pereira, L. G.; Skumryev, V. *Phys. Rev. Lett.* **2008**, *100*, 039701.
66. Harres, A.; Mikhov, M.; Skumryev, V.; de Andrade, A. M. H.; Schmidt, J. E.; Geshev, J. *Magn. Magn. Mater.* **2016**, *402*, 76.
67. Viegas, A. D.; Geshev, J.; Dorneles, L. S.; Schmidt, J. E.; Knobel, M. *J. Appl. Phys.* **1997**, *82*, 3047.
68. Masheva, V.; Grigorova, M.; Valkov, N.; Blythe, H. J.; Midlarz, T.; Blaskov, V.; Geshev, J.; Mikhov, M. *J. Magn. Magn. Mater.* **1999**, *196*, 128.
69. Santos, L. M. D.; Ligabue, R.; Dumas, A.; Roux, C. L.; Micoud, P.; Meunier, J. F.; Martin, F.; Einloft, S. *Eur. Polym. J.* **2015**, *69*, 38.